energies

MDPI

Article

Study on IMC-PID Control of Once-Through Steam Generator for Small Fast Reactor

Kai Xiao *, Yiliang Li, Pengcheng Yang, Ying Zhang, Yang Zhao and Xiaofei Pu

Science and Technology on Reactor System Design Technology Laboratory, Nuclear Power Institute of China, Chengdu 610213, China
* Correspondence: xiaokai.sky@163.com

Abstract: The simplification of simulation inevitably leads to model mismatch. In this paper, a once-through steam generator (OTSG) for a small lead bismuth fast reactor (SLBFR) is established and verified, and the OTSG model is simplified by three different methods. Based on the simplified OTSG model, IMC and IMC-PID controllers are designed to verify the sensitivity of the controller to model mismatch. The results show that the sensitivity of the controller to model mismatch is related to the filter parameters. With the increase in λ, the IMC-PID controller becomes insensitive to model mismatch caused by model linearization, non-minimum phase characteristics, noise and time delay. However, the adaptability to model mismatch sacrifices the sensitivity of the system. When λ is too large, the inertia of the controller is too large, resulting in the deterioration of the fast power regulation. Through the research of this paper, the time domain response approximation method is recommended for OTSG model simplification, and λ is recommended to be between 5 and 10 for feedwater IMC-PID controller.

Keywords: SLBFR; OTSG; IMC-PID; nonlinear; model mismatch

Citation: Xiao, K.; Li, Y.; Yang, P.; Zhang, Y.; Zhao, Y.; Pu, X. Study on IMC-PID Control of Once-Through Steam Generator for Small Fast Reactor. *Energies* **2022**, *15*, 7475. https://doi.org/10.3390/en15207475

Academic Editors: Zhe Dong, Xiaojin Huang and Xinyu Wei

Received: 22 July 2022
Accepted: 19 August 2022
Published: 11 October 2022

1. Introduction

The lead bismuth fast reactor (LBFR) has become one of the main development directions of the fourth-generation nuclear reactor because of its unique safety characteristics [1]. Nowadays, building large nuclear reactors is not a favorable option, and hence the trend for developing small nuclear reactors (SMR) is increasing correspondingly [2].

The once-through steam generator (OTSG), the key component of heat transfer in primary and secondary circuits, has been widely concerned in the small lead bismuth fast reactor (SLBFR) [3]. However, the structure of OTSG is complex, and the feedwater at the secondary side has gone through subcooled region, boiling region and superheated region, so the properties of water/steam have changed greatly. The experimental method is limited by conditions and consumes a lot of manpower and material resources [4,5]. Therefore, most scholars use numerical calculation to study OTSG. However, the drastic property changes in water/steam in OTSG bring difficulties in modeling.

Many scholars have worked to simplify the model of OTSG [6–9]. The results show that the four regions model combined with the movable boundary method has high accuracy for OTSG [10]. Unfortunately, the simplification and construction of the model make the difference between the model and the actual OTSG. Any parameter change affecting heat exchange and flow will lead to the change in feedwater demand. In addition, in order to simplify the calculation, many processes are not considered in the model. For example, factors such as the axial conduction of the tube, the heat exchange between the OTSG and the environment, etc., were not taken into account. So, the performance of the controller will worsen in industrial applications due to the model mismatch. Therefore, the robustness of the controller has also become the focus of current research [11].

Advanced control algorithms such as DMC [12] and MPC [13] have fundamentally changed the essence of PID, which will lead to new standards in safety evaluation and

many difficulties in industrial iteration. Fuzzy PID [14], Adaptive PID [15] and other PID-based control systems retain the lower logic of PID, but the parameters need to be adjusted according to the conditions, and the upper logic is still different from PID. IMC-PID calculates the parameters of PID by using the principle of IMC. It is not different from PID in application, so it is suitable for guiding and improving engineering controllers.

Garcia and Morari proposed an internal model control structure with model, control and feedback, called Internal Model Control (IMC) [16]. It has attracted extensive attention because of its simple structure and strong robustness.

In nonlinear systems, Kazantzidou et al. [17] studied the IMC for keeping and rudder roll stabilization for a surface marine craft. There is satisfactory roll reduction and the course-keeping is maintained in the presence of constant input disturbance. Singh et al. [18] designed a 2-DOF IMC-PID for power system frequency modulation, but an extra degree of freedom is fixed to cancel the sequences of the added poles of the disturbances. Therefore, what needs to be designed and calculated is still the traditional IMC. Bhattacharjee et al. [19] applied IMC to the artificial pancreas system. Through a feedforward control path to the online tuned IMC, it is proved that the online tuned IMC algorithm is able to compensate unannounced meal disorders with low infection of insulin does and reduces the risk of hyperglycemic events for different patient conditions. Li et al. [20] used the GD-DE algorithm to optimize the parameters of the IMC controller of the nonlinear uncertain aeroelastic blade system. These studies have shown that even if there is a gap between the internal model of IMC and the actual controlled object, IMC still has a relatively satisfactory performance.

In process control, Mesbahr et al. [21] present a general IMC structure with multiple degrees of freedom for the design of control systems with multiple objectives. The remarkable feature of the control structure is that the controllers can be designed independently of each other. Karan et al. [22] studied the IMC of the system with integrated time-delayed processes (ITDP), and verified the IMC through experiments such as distillation tower and liquid storage tank. The controller output is calculated by computer simulation software, which is still a certain distance from the engineering control process. Through research on the biomass boiler, Schörghuber et al. [23] found that IMC can greatly reduce the controller parameters and achieve satisfactory control performance. They promoted the industrial application of IMC through experimental research, but the inaccuracy of the model mentioned in the paper has not been studied in detail, especially when the model deviates from the steady-state point; the control effect should be the focus of future research.

In the context of nuclear reactors, Wang et al. [24] designed the IMC power controller of pressurized water reactor (PWR) and optimized the parameters by the genetic algorithm. Zeng et al. [25] designed the core power IMC-PID controller for a molten salt breeder reactor. Different from Wang's work, Zeng used the particle swarm optimization algorithm to optimize the parameters of the approximated First Order Plus Dead Time (FOPDT) model rather than the controller parameters.

Due to the security of nuclear reactors, the method of on-line parameter tuning is unrealistic, and there is a certain error between the simulation model and the actual system. The study of model mismatch has great significance for the performance of IMC and engineering applications.

On the other hand, PID is still the main controller of industry because of its simple structure. In the field with high safety requirements, the combination of PID and advanced control method is also a transition form from traditional PID to advanced control method. Therefore, it is important for engineering applications to consider the combination of advanced control methods and PID and the influence of model mismatch on the controller performance.

In this work, firstly, the model of OTSG for SLBFR is established and verified. Then, the IMC and IMC-PID controller of OTSG feedwater are designed to control the lead bismuth eutectic (LBE) outlet temperature of OTSG. The temperature control process is simplified to three FOPDT models by different methods. The effectiveness of the approximate methods

are proved by comparison with the nonlinear model. Finally, the performance of IMC-PID controller designed based on simplified FOPDT model is verified by a nonlinear model and non-minimum phase system, and the adaptability of IMC-PID to model mismatch is studied by adding nonlinear elements such as measurement noise and time delay. Finally, the performance of IMC-PID controller is studied when the model deviates from the steady state.

2. Modeling and Verification of OTSG

This section consists of two parts. In the first part, the OTSG is modeled by the moving boundary method and four region model. In the second part, the OTSG model is verified by steady-state verification, steady-state temperature distribution and transient disturbance.

2.1. Modeling of OTSG

The OTSG is used in the SLBFR. The secondary side water will change to steam in OTSG, and the heat transfer coefficient changes sharply with the change in vapor fraction. Therefore, the OTSG is divided into four regions in this work: a subcooled region, nucleate boiling region, film boiling region and superheated region. In addition, with the change in working conditions, the length of each region changes, so the movable boundary method is used. The formula derivation process of different regions and node division can be found in Ref. [26]. Therefore, in this paper, only the basic equation is given. The model was built in the MATLAB/Simulink environment. Figure 1 shows the node division diagram of OTSG, where L_c is the subcooled region, L_{b1} is the nucleate boiling region, L_{b2} is the film boiling region and L_s is the superheated region. PLS1–PLS9 are primary side LBE nodes, SSCL1–SSSL3 are secondary side water/steam nodes and $Tm1$–$Tm9$ are tube nodes.

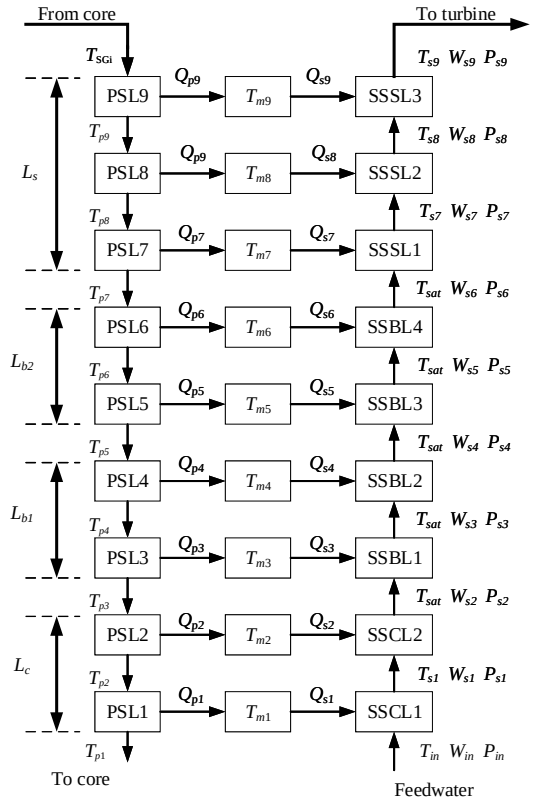

Figure 1. Node division of once-through steam generator.

The primary side, secondary side and tube can be calculated using the following formulas. Note that the primary side is liquid metal, which can be regarded as an incompressible fluid, so only energy conservation and mass conservation are considered

in the primary side. The tube does not flow, so only the energy conservation equation is considered:

$$A\left[\frac{\mathrm{d}(\overline{\rho_i}L_i)}{\mathrm{d}t}-\rho_{i+1}\frac{\mathrm{d}z_{i+1}}{\mathrm{d}t}+\rho_i\frac{\mathrm{d}z_i}{\mathrm{d}t}\right]=W_i-W_{i+1} \tag{1}$$

$$A\left[\frac{\mathrm{d}(\overline{\rho_i h_i}L_i)}{\mathrm{d}t}-\rho_{i+1}h_{i+1}\frac{\mathrm{d}z_{i+1}}{\mathrm{d}t}+\rho_i h_i\frac{\mathrm{d}z_i}{\mathrm{d}t}-L_i\frac{\mathrm{d}P_i}{\mathrm{d}t}\right]=W_i h_i-W_{i+1}h_{i+1}+Q_i \tag{2}$$

$$\frac{1}{A}\left[\frac{\mathrm{d}\overline{W_i}L_i}{\mathrm{d}t}-W_{i+1}\frac{\mathrm{d}z_{i+1}}{\mathrm{d}t}+W_i\frac{\mathrm{d}z_i}{\mathrm{d}t}\right]=P_i-P_{i+1}-\Delta P_i \tag{3}$$

where W_i is the flow rate of the i-th control body, kg/s; $\overline{\rho_i}$ is the average density of the i-th control body, kg/m^3; h is the enthalpy value, J/kg; z_i is the position of the lower boundary of the i-th control body, m; ΔP_i is the pressure drop of fluid flowing through the i-th control body, including the gravity pressure drop, friction pressure drop and acceleration pressure drop, Pa; and L is the length of the control body, m. A model with the outlet parameter as the lumped parameter has better approximation and no initial negative offset. Therefore, the OTSG is often modeled by the outlet lumped parameter method [26].

The heat transfer coefficient calculations of the four regions are summarized in Table 1.

Table 1. Heat transfer correlations in different regions.

Region	Reference	Calculation Formula
1.Subcooled region (Re ≥ 2500)	Dittus-Boelter [27]	$Nu = 0.023\mathrm{Re}^{0.8}\mathrm{Pr}^{0.4}$
1.Subcooled region (Re < 2500)	Collier [28]	$Nu = 0.17\mathrm{Re}^{0.33}\mathrm{Pr}^{0.43}(\frac{\mathrm{Pr}}{\mathrm{Pr}_w})^{0.25}Gr^{0.1}$
2.Nucleate boiling region	Chen [29]	$h = 0.023F\frac{\lambda_f^{0.6}G^{0.8}(1-x)^{0.8}Cp_f^{0.4}}{\mu_f^{0.4}D_e^{0.2}}$ $+0.00122S\frac{\lambda_f^{0.79}Cp_f^{0.45}\rho_f^{0.49}}{\sigma^{0.5}\mu_f^{0.29}h_{fg}^{0.24}\rho_g^{0.24}}\Delta T_{sat}^{0.24}\Delta P_{sat}^{0.75}$
3.Film boiling region	Miropolskiy [30]	$Nu = 0.023\{\mathrm{Re}[x+\frac{\rho_g}{\rho_f}(1-x)]\}^{0.8}\mathrm{Pr}^{0.8}Y$
4.Superheated region	Dittus-Boelter [27]	$Nu = 0.023\mathrm{Re}^{0.8}\mathrm{Pr}^{0.4}$

In Table 1, Cp is the specific heat capacity, J/°C; Pr is the Prandtl number; Re is the Reynolds number; F is the Reynolds number factor; and S is the nucleate boiling inhibition factor:

$$Y=\left[1-0.1\left(\frac{\rho_f}{\rho_g}-1\right)^{0.4}(1-x)^{0.4}\right]\left[x+\frac{\rho_f}{\rho_g}(1-x)\right]^{0.8} \tag{4}$$

$$F=\begin{cases}1.0, & X_{\mathrm{tt}}^{-1}\le 0.1\\ 2.35(X_{\mathrm{tt}}^{-1}+0.213)^{0.736}, & X_{\mathrm{tt}}^{-1}>0.1\end{cases} \tag{5}$$

$$X_{\mathrm{tt}}^{-1}=(\frac{x}{1-x})^{0.9}(\frac{\rho_f}{\rho_g})^{0.5}(\frac{\mu_g}{\mu_f})^{0.1} \tag{6}$$

$$S=\begin{cases}[1+0.12\mathrm{Re}_{\mathrm{TP}}^{1.14}]^{-1}, & \mathrm{Re}_{\mathrm{TP}}<32.5\\ [1+0.42\mathrm{Re}_{\mathrm{TP}}^{0.78}]^{-1}, & 32.5\le\mathrm{Re}_{\mathrm{TP}}<70.0\\ 0.1, & \mathrm{Re}_{\mathrm{TP}}\ge 70.0\end{cases} \tag{7}$$

$$\mathrm{Re}_{\mathrm{TP}}=\frac{G(1-x)D_e}{\mu_f}F^{1.25}\times 10^{-4} \tag{8}$$

The Nusselt number of primary LBE is calculated by the following formula [31]:

$$Nu = 4.82 + 0.0185Pe^{0.827} \tag{9}$$

where *Nu* is the Nusselt number and *Pe* is the Peclet number. The heat transfer formula of the primary side can be found in Ref. [26]. The OTSG parameters are listed in Table 2.

Table 2. The OTSG parameters.

Name	Value	Name	Value
Tube inner diameter	21 mm	Inlet LBE temperature	430 °C
Tube outer diameter	24 mm	Inlet feedwater temperature	210 °C
Length of tube	20 m	Feedwater flowrate	12.76 kg/s
Tube number	60	LBE flowrate	1767.2 kg/s

2.2. Verification

This section verifies the OTSG through steady-state parameters, steady-state temperature distribution and transient characteristics.

2.2.1. Steady State Parameters Verification

Table 3 shows the calculated and designed values of OTSG model at 100% full power (FP). It can be seen from Table 2 that the error of the outlet steam temperature is 2%, and the error of the feedwater flowrate is 1.8%, which shows that the model has high accuracy. The error of heat exchange length is 5.6%. The length of the superheated region calculated in this paper is shorter than the design value, and the steam temperature is also lower than the design value, indicating that the heat exchange coefficient calculated in this paper is less than the heat exchange coefficient used in the design. However, the error is small, which proves the accuracy of the model in this paper.

Table 3. Model calculation results at 100% FP.

Name	LBE Outlet Temperature	Steam Temperature	Feedwater Flowrate	Length of Superheated Region
Design value	320 °C	368 °C	13 kg/s	5.04 m
Calculated value	320 °C	360.8 °C	12.76 kg/s	4.76 m
Error	0	2%	1.8%	5.6%

2.2.2. Steady-State Temperature Distribution Verification

Because there are few reference data for OTST of SLBFR, we verified the rationality of this model by comparing the temperature distribution of OTSG of small PWR. Although they differ in numerical values, the regularity is consistent. The temperature distribution of OTSG at 100% FP is shown in Figure 2. Figure 3 shows the temperature distribution calculated in Ref. [32]. By comparing Figures 2 and 3, it can be found that the temperature distribution calculated in this paper is consistent with the temperature distribution calculated by RELAP5. Because the pressure loss in the flow is considered in this paper, the saturation temperature decreases slightly along the flow direction. The difference from the literature is that the primary side of this paper is LBE and the heat exchange temperature difference is also different.

2.2.3. Transient Characteristics Verification

We introduced feedwater flowrate disturbance, feedwater temperature disturbance, LBE flowrate disturbance and LBE inlet temperature disturbance to OTSG, and observed the change in LBE outlet temperature, as shown in Figure 4. The disturbance of feedwater flowrate and LBE flowrate is −5% at the rate of −2.45%/s, and the disturbance of feedwater temperature and LBE temperature is −5 °C at the rate of −3.5 °C/s. All disturbances are introduced in 20 s, and the system was 100% FP before the disturbance. It can be seen from Figure 4 that the feedwater temperature has the least impact on the LBE outlet temperature. The feedwater flowrate, LBE flowrate and LBE inlet temperature disturbances change the LBE temperature by +3.72 °C, −4.21 °C and −3.46 °C, respectively.

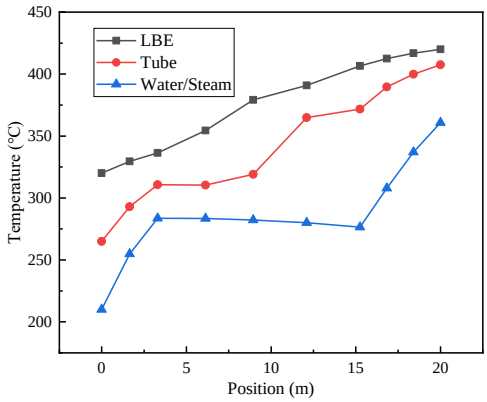

Figure 2. Temperature distribution of OTSG in this work.

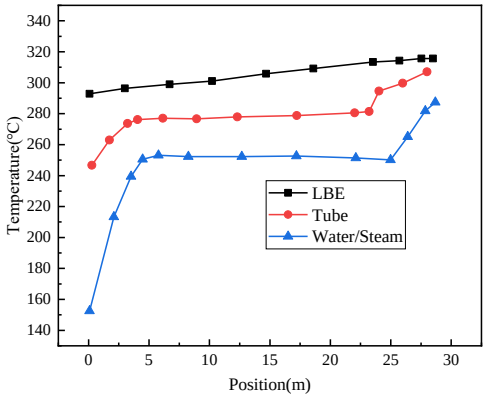

Figure 3. Temperature distribution of OTSG in Ref. [28].

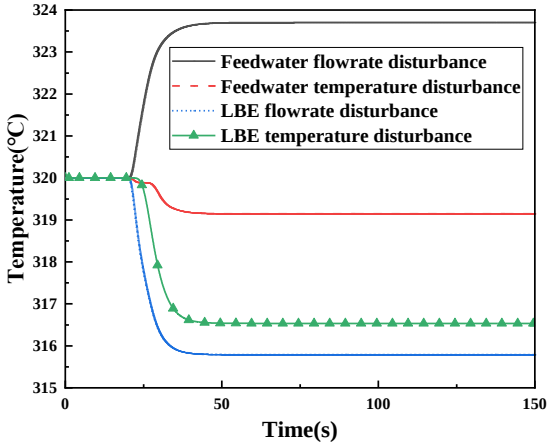

Figure 4. LBE outlet temperature variation under different disturbances.

Ref. [28] gives the characteristics of the system when four step disturbances are introduced. In this paper, the ramp signal is used for the consistency of the content of the article. The content of the step disturbances can be found in Appendix A. Through the comparison with the reference, it can be found that the law of this paper is consistent with the reference and conforms to the objective law.

3. Controller Design and Simulation Platform Development

The LBE corrosivity causes the LBE flowrate change to be restricted by the primary loop, so it is not the best solution to adjust the LBE outlet temperature through the LBE

flowrate. Adjusting the LBE outlet temperature through feedwater temperature must consider the rate of temperature change. Due to the large heat capacity of water and the faster response of the OTSG, adjusting the LBE outlet temperature through feedwater temperature cannot meet the needs of OTSG. The feedwater flowrate can be regulated by valves or pumps quickly, which is the best choice to control the LBE outlet temperature. Therefore, a flowrate controller is designed in this section.

This section contains two parts. Firstly, the principle and design method of IMC controller are introduced. Through the analysis of the characteristics of IMC, the IMC-PID is introduced, and the design method of IMC-PID controller is introduced.

3.1. IMC

IMC is a control method based on internal model. Figure 5 shows the general structure of the IMC controller, where G_c is the IMC controller, G is the controlled object, G_m is the nominal model (internal model), Y is the output of the controlled object, D is the disturbance (including measurement noise) and R is the reference of Y. The output of the system can be expressed as:

$$Y(s) = \frac{G_c(s)G(s)}{1 + G_c(s)(G(s) - G_m(s))}R(s) + \frac{1 - G_c(s)G_m(s)}{1 + G_c(s)(G(s) - G_m(s))}D(s) \tag{10}$$

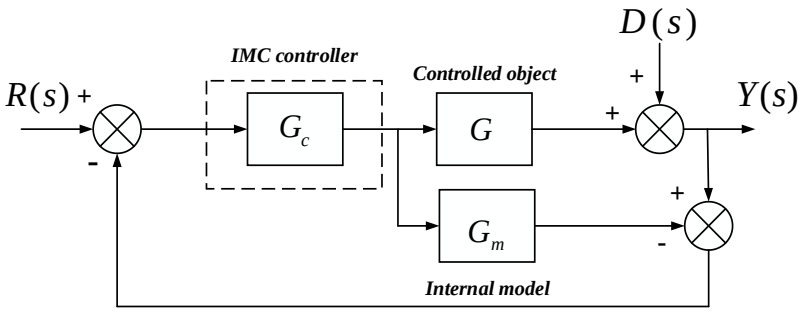

Figure 5. General structure of IMC.

It is not difficult to see from Equation (5) that when $G_cG_m = 1$, the system will achieve adequate anti-disturbance performance. At this time, if $G_m = G$, the system also has suitable tracking performance. Therefore, the controller is designed as follows:

Step 1: Let $G_c(s) = G_m^{-1}(s)$. When $G_m(s)$ has zeros in the right half plane of complex plane, $G_c(s)$ will be unstable and difficult to achieve in engineering. So, $G_m(s)$ can be expressed as:

$$G_m(s) = G_m^+(s)G_m^-(s) \tag{11}$$

$$G_c(s) = \left[G_m^-(s)\right]^{-1} \tag{12}$$

where $G_m^+(s)$ is the non-minimum phase element of $G_m(s)$ and $G_m^-(s)$ is the minimum phase part of $G_m(s)$.

Step 2: If $G_m^-(s)$ is regular, then $G_c(s)$ must be non-strictly regular. The robustness of IMC can be improved by including a low pass filter:

$$G_c(s) = \frac{1}{(1 + \lambda s)^n}\left[G_m^-(s)\right]^{-1} \tag{13}$$

where n is the order of the filter to ensure the regularity of $G_c(s)$, so n depends on $G_m^-(s)$, and this parameter does not need to be tuned; λ is a filter constant, which needs to be tuned for IMC. It can be seen from Equation (13) that only λ needs to be tuned.

According to the OTSG model established in Section 2, the transfer function from feedwater flow to outlet LBE temperature can be obtained. Due to the high order, the

dominant pole method is used to reduce the order of the transfer function, and the reduced transfer function is (only 100% FP is given here, and other power levels can be found in the Appendix A):

$$G_{100,r} = \frac{-0.1482s^3 - 1.417s^2 - 0.841s - 1.121}{s^4 + 2.064s^3 + 2.13s^2 + 1.201s + 0.2044} \tag{14}$$

$G_c(s)$ designed according to the above steps is (λ = 1 here, and the other calculation results can be found in the Appendix A):

$$G_c(s) = \frac{-s^4 - 2.064s^3 - 2.13s^2 - 1.201s - 0.2044}{0.1482s^4 + 1.565s^3 + 2.258s^2 + 1.962s + 1.121} \tag{15}$$

The step change in LBE outlet temperature reference is from 320 °C to 325 °C at 20 s. Figure 6 shows the performance of IMC with different controller parameters. Compared with PID, IMC parameter tuning is simple and clear. Single parameter adjustment avoids the possibility of more combinations. It can be seen from Figure 6 that the impact of λ on performance is intuitive. With the increase in λ, the response of the system becomes slower, but a small λ will cause the controller output to be aggressive.

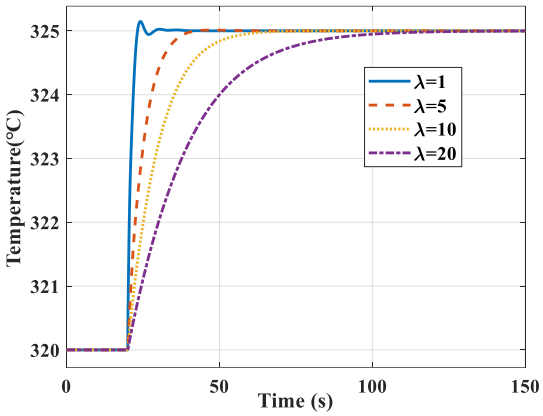

Figure 6. Control performance of IMC with different parameters.

In addition, it can be seen from Equation (15) that the order of IMC is higher than PID. With simple structure, principle and suitable control effect, traditional PID has become the most important controller in industry. So, combining the advantages of IMC and the easy implementation of PID is also an important direction of industrial controller research.

3.2. IMC-PID

The structure of the IMC-PID controller is shown in Figure 7. Obviously, when C in Figure 7 is PID controller, Figure 7 is transformed into traditional PID closed-loop control. Therefore, the key idea of the IMC-PID controller is to convert C into PID equivalently.

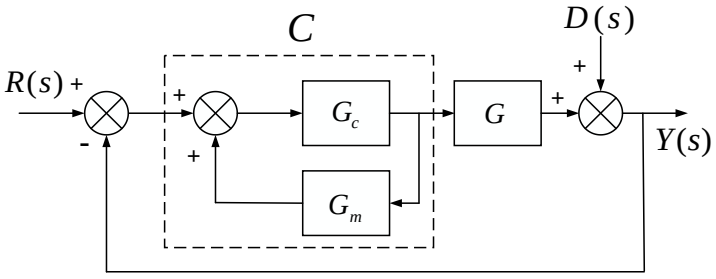

Figure 7. General structure of IMC-PID controller.

From Figure 7, the transfer function of C can be obtained as:

$$C(s) = \frac{G_c(s)}{1 - G_c(s)G_m(s)} = \frac{[G_m^-(s)]^{-1}}{(1+\lambda s)^n - G_m^+(s)} \tag{16}$$

The transfer function of traditional PID can be expressed as:

$$C_{PID}(s) = K_p + \frac{K_i}{s} + \frac{K_d s}{T_d s + 1} = \frac{(K_p T_d + K_d)s^2 + (K_p + K_i T_d)s + K_i}{s(T_d s + 1)} \tag{17}$$

where K_p, K_i and K_d are the coefficients of proportional, integral and differential elements, respectively. Since the differential element is difficult to realize, the third term in Equation (17) is usually used to approximate the ideal differential element, and T_d is the filter constant.

Usually, most of the controlled objects in industry can be represented by the FOPDT system, which can be expressed as follows:

$$G_r(s) = \frac{K}{Ts + 1} e^{-\theta s} \tag{18}$$

The approximation process will bring errors to the model and make $G_m(s)$ deviate from G. Therefore, in order to study the influence of model deviation on the effect of IMC-PID control, three different methods are used to approximate the transfer function.

3.2.1. Approximate Method of FOPDT

Method 1: Time domain response approximation method. By introducing the step signal and analyzing the output, the transfer function of the approximate FOPDT of the system is obtained. From Equation (18), the response of the system in the time domain can be derived:

$$\widetilde{y} = \begin{cases} K(1 - e^{-(\frac{t-\theta}{T})}), & t > \theta \\ 0, & t \le \theta \end{cases} \tag{19}$$

When $s = 0$, $K = G(0)$ can be obtained from $G(0) = G'(0)$. Then, by comparing the nonlinear model output y with the approximate model output $\widetilde{y}$, the parameters θ and T are identified.

Method 2: Derivative calculation method. The first and second derivatives of Equation (18) for s are obtained:

$$\frac{G_r'(s)}{G_r(s)} = -\theta - \frac{T}{1 + Ts} \tag{20}$$

$$\frac{G_r''(s)}{G_r(s)} - \left(\frac{G_r'(s)}{G_r(s)}\right)^2 = \frac{T^2}{(1 + Ts)^2} \tag{21}$$

Substitute $s = 0$ into $G(s)$ and $G_r(s)$. Then, the left side of Equations (20) and (21) are equivalent as follows:

$$\frac{G'(0)}{G(0)} = \frac{G_r'(0)}{G_r(0)} = -\theta - T = -T_{ar} \tag{22}$$

$$\frac{G''(0)}{G(0)} = \frac{G_r''(0)}{G_r(0)} = T^2 + T_{ar}^2 \tag{23}$$

where the purpose of dividing $G(0)$ is to eliminate $e^{-\theta s}$; the calculation method of K is the same as Method 1.

Method 3: Suboptimal order reduction method. This method can be obtained from Ref. [33] and is not introduced here.

The transfer functions from feedwater flowrate to LBE outlet temperature approximated by three methods at 100% FP are shown in Table 4. The transfer functions at the remaining power levels can be found in Appendix A.

Table 4. Approximated transfer functions by different methods.

Name	Method 1	Method 2	Method 3
$G_r(s)$	$\frac{-5.496}{4.527s+1}e^{-0.91s}$	$\frac{-5.496}{4.055s+1}e^{-1.11s}$	$\frac{-5.496}{4.334s+1}e^{-0.967s}$
$G_d(s)$	$\frac{-5.496(1-0.455s)}{(4.527s+1)(1+0.455s)}$	$\frac{-5.496(1-0.555s)}{(4.055s+1)(1+0.555s)}$	$\frac{-5.496(1-0.4835s)}{(4.055s+1)(1+0.4835s)}$

The OTSG operates stably at 100% FP at t = 0. Then, the feedwater flowrate step changes +1% and +5% at t = 20 s. Figure 8 shows the output of nonlinear model, reduced order model and transfer function listed in Table 4. It can be seen from Figure 8 that the outputs of the models calculated by the three methods are consistent with the nonlinear model. Since the three methods calculate K in the same way, the steady-state values of the three methods are equal. Comparing Figure 8a,b, it can be found that the difference between the linear model and the nonlinear model increases with the deviation broadening from the steady state. The comparison showed that the output of Method 1 is closest to the nonlinear model, easy to calculate, and can be calculated by transfer function or fitted by system response curve, which is more convenient for engineering applications. Therefore, Method 1 is recommended. Ref. [34] also provides a method to approximate the frequency domain characteristics of the system, but this method is limited by the characteristics of the controlled object and the calculation is complex, so it will not be introduced here.

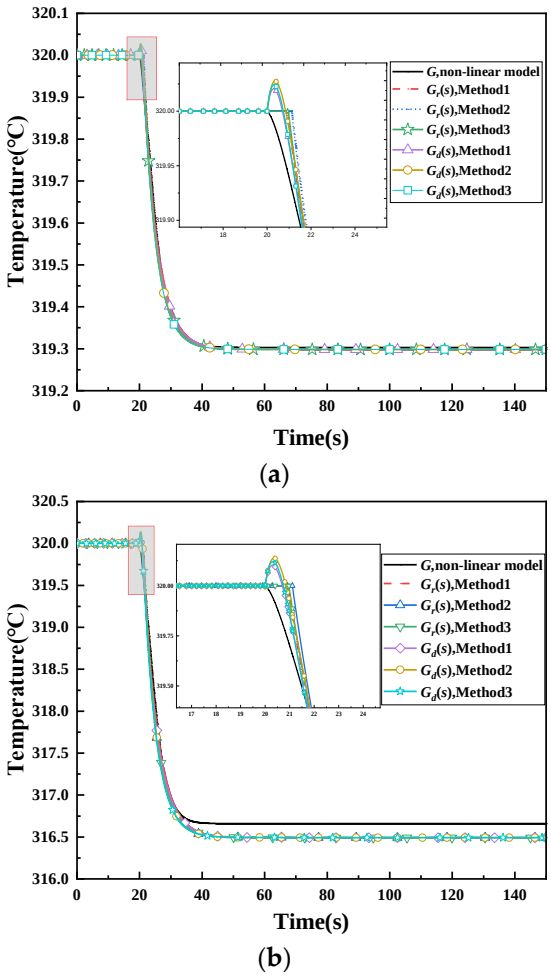

Figure 8. Comparison between simplified model and nonlinear model: (**a**) +1% feedwater flowrate disturbance, (**b**) +5% feedwater flowrate disturbance.

3.2.2. Design of IMC-PID Controller

The approximate analysis of time delay terms is performed by the Pade method [25]:

$$e^{-\theta s} = \frac{1 - \frac{\theta}{2}s}{1 + \frac{\theta}{2}s} \tag{24}$$

So, the IMC-PID controller is designed according to the method in Section 3.1:

$$G_d(s) = \frac{K}{Ts + 1} \frac{1 - \frac{\theta}{2}s}{1 + \frac{\theta}{2}s} \tag{25}$$

$$G_m^- = \frac{K}{Ts + 1}, \qquad G_m^+ = \frac{1 - \frac{\theta}{2}s}{1 + \frac{\theta}{2}s} \tag{26}$$

$G_d(s)$ calculated by the three methods is summarized in Table 4. Then, substitute Equation (26) into Equation (16):

$$C(s) = \frac{\frac{1}{K(\theta+\lambda)}(Ts + 1)(1 + \frac{\theta}{2}s)}{s\left[\frac{\theta\lambda}{2(\theta+\lambda)}s + 1\right]} \tag{27}$$

The parameters of the IMC-PID controller can be obtained by comparing Equations (27) and (17):

$$\begin{cases} T_d = \frac{\lambda\frac{\theta}{2}}{\lambda+\frac{\theta}{2}} \\ K_i = \frac{1}{K(\lambda+\theta)} \\ K_p = K_i(T + \frac{\theta}{2} - T_d) \\ K_d = \frac{T\frac{\theta}{2}}{K(\lambda+\theta)} - K_p T_d \end{cases} \tag{28}$$

The parameters calculated by the three methods with λ = 1 are listed in Table 5.

Table 5. IMC-PID controller parameters (λ = 1).

Name	Method 1	Method 2	Method 3
T_d	0.2382	0.2630	0.2458
K_p	−0.4519	−0.3748	−0.4229
K_i	−0.0953	−0.0862	−0.0925
K_d	−0.0886	−0.0955	−0.0899

3.3. Simulation Platform

MATLAB/Simulink is used to build the OTSG model and controller model. Figure 9 shows the structure of the OTSG feedwater control simulation platform. In Figure 9, module 1 is the reference, module 2 is IMC-PID controller, module 3 is IMC controller, module 4 is OTSG nonlinear model G, module 5 is FOPDT model $G_r(s)$, module 6 is non-minimum phase model $G_d(s)$, module 7 is noise and switch and the module 8 is time delay and switch.

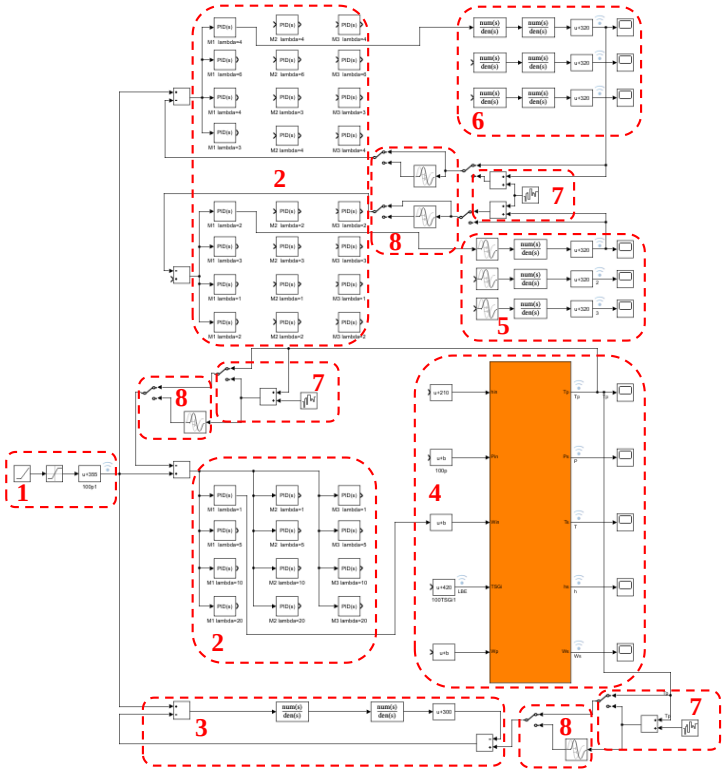

Figure 9. Structure of the OTSG feedwater control simulation platform.

4. Results and Discussion

This section verifies the adaptability of IMC-PID to model mismatch under different controller parameters through four ways. Section 4.1 tests the impact of three different approximation methods on IMC-PID. Section 4.2 studies the performance of IMC-PID through the nonlinear model and non-minimum phase system. Section 4.3 studies the performance of IMC-PID under different parameters. In Section 4.4, the adaptability of IMC-PID to the time delay element under different parameters is studied. In Section 4.5, the tracking ability of different controller parameters is studied through rapid load reduction.

4.1. Effect of Different Control Parameters

The step change in LBE outlet temperature reference is from 320 °C to 325 °C at 20 s, and the influence of different λ values on the performance of IMC-PID controller is studied by comparing the system output. Figure 10 shows the control performance of IMC and IMC-PID controller with different parameters.

It can be seen from Figure 10 that with the increase in λ, the adjustment time of the system gradually increases. At the same time, the output of IMC and IMC-PID are closer. This shows that as λ increases, the robustness of the system gradually increases and the sensitivity to model mismatch gradually decreases.

It can be seen from Equation (14) that the filtering element introduces a pole with a value of $-\frac{1}{\lambda}$ and as the λ increases, the pole approaches the origin. This leads to the more obvious influence of pole $-\frac{1}{\lambda}$ on the system with the increase in λ, and gradually becomes the dominant pole of the system. Therefore, when λ is large, IMC-PID has the same performance with IMC.

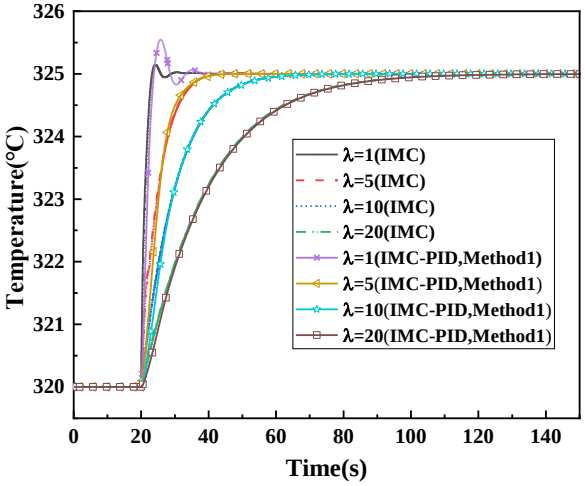

Figure 10. Comparison of IMC and IMC-PID performance under different parameters.

Figure 11 shows the performance of IMC-PID controller parameters calculated by three methods. It can be seen from Figure 11 that the performance of the IMC-PID controller obtained by the three methods gradually disappears with the increase in λ. The results are consistent with those in Figure 8, which show that with the increase in λ, the system will become insensitive to model mismatch.

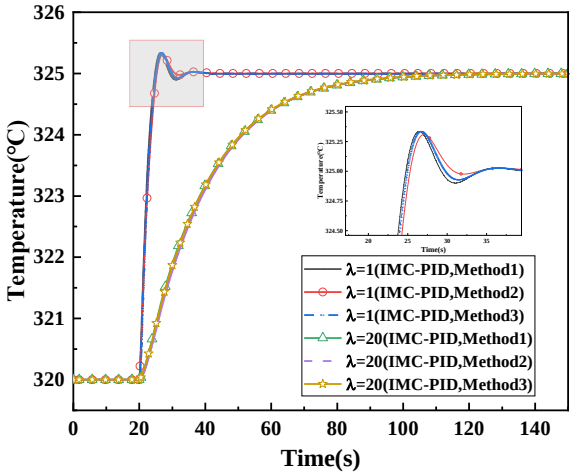

Figure 11. Comparison of IMC-PID performance of different methods.

As can be seen in Figure 11, the transfer functions obtained by the three approximate methods can describe the characteristics of the system approximately, and the performance of the controllers designed by the three methods is not different, especially when λ is large. Therefore, the results of Method 1 are used for subsequent analysis in this paper.

4.2. Effect of Model Mismatch

According to the established controlled object, the controller performance will be poor due to the model mismatch in practical application. Therefore, it is important to study the influence of the controller parameters on model mismatch. It may be assumed that the nonlinear model G established in Section 2.1 is the actual controlled object 1, $G_d(s)$ in Table 4 is the actual controlled object 2, and $G_r(s)$ is the model established by simulation calculation. $G_r(s)$ ignores the nonlinearity of G and the non-minimum phase characteristics in $G_d(s)$.

Unfortunately, industrial processes use the system identification method to obtain the system transfer function and design the controller. At the same time, for the convenience of

controller design, the system is usually approximated as FOPDT, such as $G_r(s)$, to replace G, thereby ignoring the nonlinearity of original system G and the non-minimum phase characteristic of $G_d(s)$. This is consistent with our assumption.

Figure 12 shows the control performance of IMC and IMC-PID on models $G_d(s)$ under different parameters when the LBE outlet temperature reference of the OTSG has a +5 °C step change. The control performance of IMC-PID on nonlinear model G is shown in Figure 10.

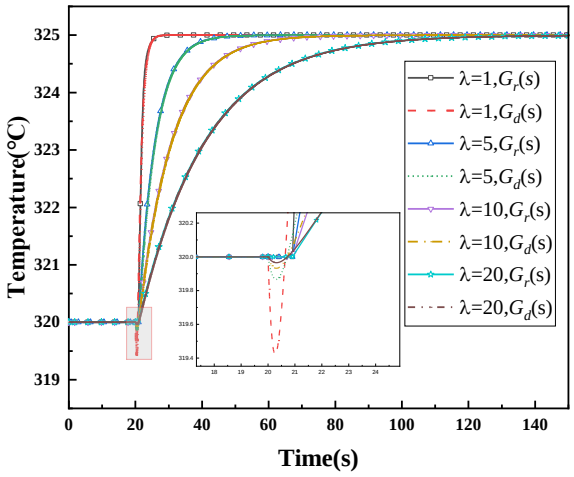

Figure 12. Performance of IMC-PID on different controlled objects.

By comparing Figures 10 and 12, it can be found that the approximation of the time delay element using first-order Pade is very effective in Section 3.2.2. When the controlled object is a minimum phase system, IMC-PID can realize fast regulation without overshoot. When the controlled object is a non-minimum phase system, the control performance of IMC-PID deteriorates slightly. With the increase in λ, the output of IMC-PID controller is gradually conservative and insensitive to non-minimum phase characteristics. It can be seen from Figure 10 that with the increase in λ, the system is also no longer sensitive to the disturbance of the internal model (model mismatch and non-minimum phase characteristics).

4.3. Effect of Measurement Noise on Control Performance

To simulate the sensor measurement noise, 0.25% of the measurement noise is added to the output of the controlled object. Figure 13 shows the performance of IMC-PID under different control parameters. As can be seen from Figure 13, when λ = 1, the system responds quickly, but it is also more sensitive to measurement noise. When λ = 20, the measurement noise has little effect on the performance of the IMC-PID controller. The effect of the controller on G, $G_r(s)$ and $G_d(s)$ is consistent. In addition, the results show that the PID controller with appropriate parameters can also achieve the effect of disturbance rejection. Moreover, λ plays the same role in IMC and IMC-PID controller. Therefore, tuning the PID controller by the IMC method is helpful for practical applications. Three parameters of PID that need to be tuned are simplified to one, which is convenient for design and tuning.

4.4. Influence of Time Delay Element

Based on Section 4.3, a time delay element is added to simulate the time of signal transmission and controller output. Figure 14 shows the performance of the IMC-PID controller with different parameters when there is a 1 s delay from error generation to controller output.

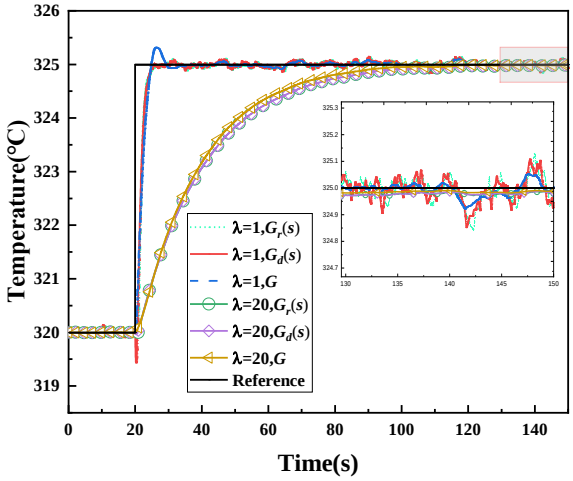

Figure 13. Influence of noise on different controller parameters.

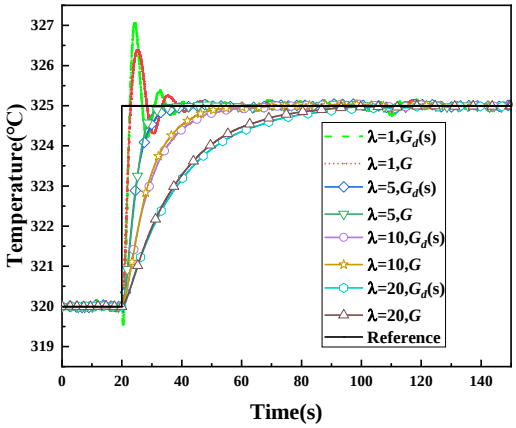

Figure 14. Influence of delay on different controller parameters.

It can be seen from Figure 14 that when λ = 1, the performance of the controller is further deteriorated than in Figure 11, resulting in large overshoot. Comparing Figures 10–14, it can be found that the smaller filter parameters are sensitive to model mismatch caused by nonlinear elements, non-minimum phase elements, noise and time delay, which can be regarded as the model mismatch between the actual model and the simulation model for controller design. It can be found that the larger filter parameters sacrifice certain sensitivity, but the robustness is strengthened. From Figure 14, it can be found that the impact of the introduced element in this paper on the performance of IMC-PID with λ = 20 can be ignored. Therefore, if there is a model mismatch problem in the controller design, it is inappropriate to only use load tracking as the evaluation index of the controller, and the optimization of the controller is likely to be futile.

Although the increase in λ will make the IMC-PID controller insensitive to model mismatch, it will also cause the controller output to be too conservative, resulting in poor control performance.

4.5. Rapid Power Changes

Rapid power changes usually occur in load rejection or emergency shutdown conditions. In these conditions, the powers of the primary and secondary loops of the nuclear reactor are reduced at the same time. Therefore, the input of OTSG and the reference change at the same time. This section simulates a rapid power drop from 100% FP to 30% FP. The change in LBE inlet temperature of OTSG due to the simultaneous power reduction on the primary side is shown in Figure 15. At the same time, the OTSG feedwater

control system needs to control the LBE outlet temperature to a reference curve to prevent the coolant temperature from introducing reactivity and causing the core power to change. The reference of LBE outlet temperature is shown in Figure 15.

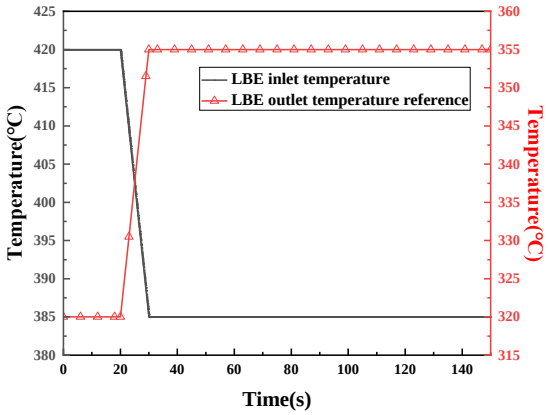

Figure 15. Change in LBE temperature at OTSG inlet during load shedding.

Figure 16 also shows the performance under different controller parameters. It can be seen from Figure 16 that when λ = 20, the system output fluctuates for a period of time, and even lower than the initial temperature. The reason is that the LBE flow velocity is restricted due to the corrosiveness. The change in LBE inlet temperature takes time to change the outlet temperature. As shown in Figure 4, there is an obvious delay in the influence of LBE inlet temperature on LBE outlet temperature. At this time, the change in controller reference reduces the feedwater flowrate to increase the LBE outlet temperature. Subsequently, the influence of LBE inlet temperature change is transmitted to the OTSG outlet, resulting in the decrease in LBE outlet temperature, while the output of λ controller is smaller and the LBE temperature decreases. When the λ is small, the output of the system is large, and the disturbance of LBE at the inlet becomes less obvious. We can observe that the slopes of the four curves in Figure 16 change at 30 s.

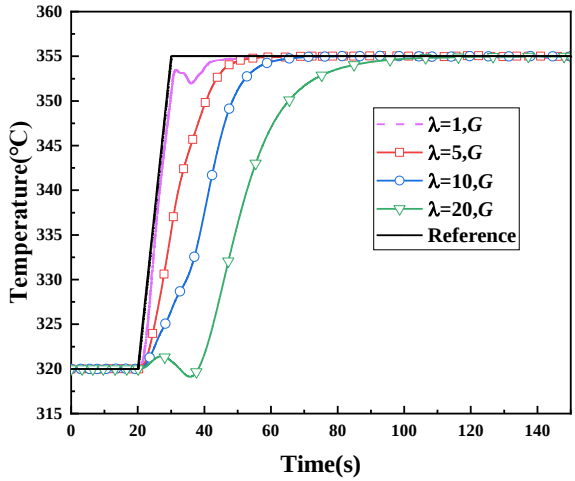

Figure 16. Performance of different controller parameters in rapid power reduction.

Based on the research of this paper, λ of IMC-PID feedwater controller for the presented OTSG of SLBFR is recommended to be between 5 and 10. This research on model mismatch has universality, and this method can be used to initialize other PID controller parameters in industrial processes.

5. Conclusions

We mainly studied the control effect of IMC-PID when the OTSG model is mismatched. By introducing different disturbances, the control performance was tested and the following results were obtained:

1. It is feasible to simplify the OTSG model to the FOPDT model and design an IMC-PID controller. As the system deviates from the steady-state point, the approximate model error gradually increases.
2. The research on a nonlinear model, non-minimum phase system, system with measurement noise, time delay and large range power regulation shows that with the increase in λ, the robustness of the IMC-PID controller is enhanced, but the response of the system is slow.
3. PID controllers have the ability of disturbance rejection (noise and model mismatch), but there is no guidance for parameter setting. Therefore, it is simple and effective to adjust PID parameters by the IMC-PID method.
4. We recommend that the λ of OTSG feedwater IMC-PID controller be between 5 and 10 to ensure the load tracking ability and robustness.

Author Contributions: Conceptualization, K.X.; methodology, K.X.; software, K.X. and Y.L.; validation, K.X. and Y.L.; formal analysis, P.Y.; investigation, P.Y.; resources, Y.Z. (Ying Zhang); data curation, Y.Z. (Ying Zhang); writing—original draft preparation, K.X.; writing—review and editing, Y.Z. (Yang Zhao) and X.P.; visualization, Y.Z. (Yang Zhao); supervision, K.X.; project administration, K.X.; funding acquisition, K.X. All authors have read and agreed to the published version of the manuscript.

Funding: This research is supported by the Innovative Scientific Program of CNNC.

Acknowledgments: Innovative Scientific Program of CNNC.

Conflicts of Interest: The authors declare no conflict of interest.

Appendix A

Feedwater flowrate disturbance, feedwater temperature disturbance, LBE flowrate disturbance and LBE inlet temperature disturbance are introduced to OTSG, and the changes in LBE outlet temperature are observed. Figure A1 shows the change in LBE outlet temperature under different disturbances. The disturbance of feedwater flowrate and LBE flowrate is step change −5%, and the disturbance of feedwater temperature and LBE temperature is step change −5 °C. All disturbances are introduced in 20 s, and the system was 100% FP before the disturbance.

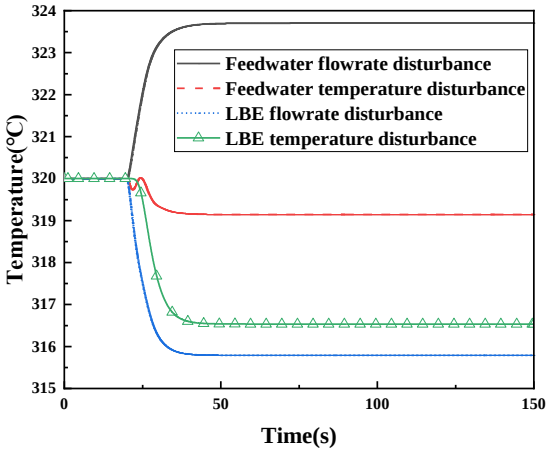

Figure A1. LBE outlet temperature variation under different step disturbances.

Figure A2 shows the change in primary side outlet temperature under different disturbances in Ref. [23]. The disturbance of feedwater flowrate is step change −2.3%, and the disturbance of feedwater temperature and primary side temperature is step change −5 °C. Comparing Figures A1 and A2, it can be seen that the model in this work is consistent with the RELAP5 model in Ref. [23]. The effect of feedwater flowrate disturbance in the reference is less than our model, because the feedwater flowrate disturbance introduced in the reference is only 2.3% and that in this paper is 5%.

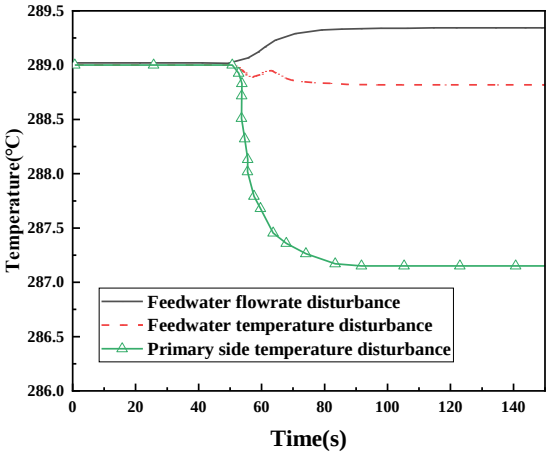

Figure A2. Primary side outlet temperature under different step disturbances in Ref. [23].

Transfer functions of 100%, 70%, 50% and 30% FP are as follows (the input is feedwater flow (kg/s) and the output is LBE outlet temperature of OTSG (°C)):

100% FP:

$$G_{100} = \frac{-321.7s^{43}-9.927e06s^{42}-1.108e11s^{41}-5.297e14s^{40}-1.013e18s^{39}-8.877e20s^{38}-3.761e23s^{37}-8.337e25s^{36}-}{s^{45}+3.236e04s^{44}+3.911e08s^{43}+2.174e12s^{42}+5.729e15s^{41}+7.957e18s^{40}+6.083e21s^{39}+2.53e24s^{38}+5.567e26s^{37}+7.331e28s^{36}+}$$
$$\frac{1.113e28s^{35}-9.927e29s^{34}-6.341e31s^{33}-3.051e33s^{32}-1.146e35s^{31}-3.45e36s^{30}-8.498e37s^{29}-1.739e39s^{28}-2.994e40s^{27}-4.376e41s^{26}-}{6.396e30s^{35}+3.972e32s^{34}+1.849e34s^{33}+6.687e35s^{32}+1.932e37s^{31}+4.553e38s^{30}+8.891e39s^{29}+1.457e41s^{28}+2.024e42s^{27}+2.402e43s^{26}+}$$
$$\frac{5.473e42s^{25}-5.892e43s^{24}-5.485e44s^{23}-4.433e45s^{22}-3.119e46s^{21}-1.914e47s^{20}-1.026e48s^{19}-4.809e48s^{18}-1.971e49s^{17}-7.065e49s^{16}-}{2.452e44s^{25}+2.162e45s^{24}+1.654e46s^{23}+1.101e47s^{22}+6.393e47s^{21}+3.243e48s^{20}+1.438e49s^{19}+5.583e49s^{18}+1.896e50s^{17}+5.635e50s^{16}+}$$
$$\frac{2.213e50s^{15}-6.05e50s^{14}-1.442e51s^{13}-2.987e51s^{12}-5.366e51s^{11}-8.325e51s^{10}-1.11e52s^{9}-1.263e52s^{8}-1.217e52s^{7}-9.815e51s^{6}-}{1.463e51s^{15}+3.317e51s^{14}+6.55e51s^{13}+1.124e52s^{12}+1.669e52s^{11}+2.134e52s^{10}+2.337e52s^{9}+2.173e52s^{8}+1.697e52s^{7}+1.096e52s^{6}+}$$
$$\frac{6.512e51s^{5}-3.47e51s^{4}-1.431e51s^{3}-4.287e50s^{2}-8.322e49s-7.924e48}{5.746e51s^{5}+2.373e51s^{4}+7.41e50s^{3}+1.636e50s^{2}+2.259e49s+1.442e48}$$

70% FP:

$$G_{70} = \frac{-312.9s^{43}-9.514e06s^{42}-1.047e11s^{41}-4.941e14s^{40}-9.374e17s^{39}-8.059e20s^{38}-3.272e23s^{37}-6.876e25s^{36}-}{s^{45}+3.194e04s^{44}+3.815e08s^{43}+2.103e12s^{42}+5.53e15s^{41}+7.666e18s^{40}+5.816e21s^{39}+2.364e24s^{38}+4.912e26s^{37}+5.926e28s^{36}+}$$
$$\frac{8.593e27s^{35}-7.079e29s^{34}-4.143e31s^{33}-1.817e33s^{32}-6.205e34s^{31}-1.698e36s^{30}-3.801e37s^{29}-7.079e38s^{28}-1.111e40s^{27}-1.484e41s^{26}-}{4.629e30s^{35}+2.541e32s^{34}+1.039e34s^{33}+3.296e35s^{32}+8.362e36s^{31}+1.735e38s^{30}+2.994e39s^{29}+4.354e40s^{28}+5.392e41s^{27}+5.733e42s^{26}+}$$
$$\frac{1.7e42s^{25}-1.681e43s^{24}-1.443e44s^{23}-1.078e45s^{22}-7.035e45s^{21}-4.017e46s^{20}-2.01e47s^{19}-8.819e47s^{18}-3.392e48s^{17}-1.144e49s^{16}-}{5.265e43s^{25}+4.199e44s^{24}+2.92e45s^{23}+1.775e46s^{22}+9.46e46s^{21}+4.425e47s^{20}+1.819e48s^{19}+6.574e48s^{18}+2.088e49s^{17}+5.829e49s^{16}+}$$
$$\frac{3.375e49s^{15}-8.703e49s^{14}-1.957e50s^{13}-3.829e50s^{12}-6.492e50s^{11}-9.5e50s^{10}-1.193e51s^{9}-1.278e51s^{8}-1.156e51s^{7}-8.728e50s^{6}-}{1.428e50s^{15}+3.063e50s^{14}+5.741e50s^{13}+9.374e50s^{12}+1.327e51s^{11}+1.621e51s^{10}+1.695e51s^{9}+1.505e51s^{8}+1.12e51s^{7}+6.892e50s^{6}+}$$
$$\frac{5.402e50s^{5}-2.673e50s^{4}-1.018e50s^{3}-2.806e49s^{2}-5.016e48s-4.45e47}{3.43e50s^{5}+1.341e50s^{4}+3.951e49s^{3}+8.181e48s^{2}+1.047e48s+5.984e46}$$

50% FP:

$$G_{50} = \frac{-289.5s^{43}-8.822e06s^{42}-9.737e10s^{41}-4.627e14s^{40}-8.922e17s^{39}-7.751e20s^{38}-3.139e23s^{37}-6.648e25s^{36}-}{s^{45}+3.204e04s^{44}+3.842e08s^{43}+2.133e12s^{42}+5.687e15s^{41}+8.006e18s^{40}+6.158e21s^{39}+2.524e24s^{38}+5.225e26s^{37}+6.204e28s^{36}+}$$
$$\frac{8.402e27s^{35}-6.986e29s^{34}-4.105e31s^{33}-1.796e33s^{32}-6.081e34s^{31}-1.641e36s^{30}-3.609e37s^{29}-6.579e38s^{28}-1.008e40s^{27}-1.312e41s^{26}-}{4.72e30s^{35}+2.505e32s^{34}+9.859e33s^{33}+3.003e35s^{32}+7.3e36s^{31}+1.45e38s^{30}+2.396e39s^{29}+3.337e40s^{28}+3.959e41s^{27}+4.037e42s^{26}+}$$
$$\frac{1.462e42s^{25}-1.406e43s^{24}-1.172e44s^{23}-8.504e44s^{22}-5.391e45s^{21}-2.991e46s^{20}-1.455e47s^{19}-6.205e47s^{18}-2.322e48s^{17}-7.62e48s^{16}-}{3.561e43s^{25}+2.732e44s^{24}+1.831e45s^{23}+1.075e46s^{22}+5.544e46s^{21}+2.516e47s^{20}+1.006e48s^{19}+3.545e48s^{18}+1.101e49s^{17}+3.009e49s^{16}+}$$
$$\frac{2.19e49s^{15}-5.504e49s^{14}-1.207e50s^{13}-2.304e50s^{12}-3.812e50s^{11}-5.445e50s^{10}-6.677e50s^{9}-6.979e50s^{8}-6.157e50s^{7}-4.525e50s^{6}-}{7.236e49s^{15}+1.527e50s^{14}+2.819e50s^{13}+4.537e50s^{12}+6.336e50s^{11}+7.631e50s^{10}+7.866e50s^{9}+6.874e50s^{8}+5.03e50s^{7}+3.033e50s^{6}+}$$
$$\frac{2.721e50s^{5}-1.303e50s^{4}-4.774e49s^{3}-1.258e49s^{2}-2.127e48s-1.754e47}{1.475e50s^{5}+5.622e49s^{4}+1.608e49s^{3}+3.222e48s^{2}+3.985e47s+2.225e46}$$

30% FP:

$$G_{30} = \frac{-201.3s^{43}-6.149e06s^{42}-6.769e10s^{41}-3.187e14s^{40}-6.026e17s^{39}-5.137e20s^{38}-2.088e23s^{37}-4.77e25s^{36}-}{s^{45}+3.214e04s^{44}+3.853e08s^{43}+2.129e12s^{42}+5.635e15s^{41}+7.874e18s^{40}+6.028e21s^{39}+2.474e24s^{38}+5.187e26s^{37}+6.256e28s^{36}+}$$
$$\frac{6.759e27s^{35}-6.346e29s^{34}-4.167e31s^{33}-2.009e33s^{32}-7.404e34s^{31}-2.152e36s^{30}-5.054e37s^{29}-9.777e38s^{28}-1.58e40s^{27}-2.159e41s^{26}-}{4.828e30s^{35}+2.595e32s^{34}+1.033e34s^{33}+3.175e35s^{32}+7.782e36s^{31}+1.557e38s^{30}+2.587e39s^{29}+3.62e40s^{28}+4.312e41s^{27}+4.41e42s^{26}+}$$
$$\frac{2.513e42s^{25}-2.51e43s^{24}-2.162e44s^{23}-1.612e45s^{22}-1.043e46s^{21}-5.872e46s^{20}-2.878e47s^{19}-1.229e48s^{18}-4.571e48s^{17}-1.481e49s^{16}-}{3.898e43s^{25}+2.995e44s^{24}+2.009e45s^{23}+1.18e46s^{22}+6.081e46s^{21}+2.756e47s^{20}+1.099e48s^{19}+3.857e48s^{18}+1.191e49s^{17}+3.23e49s^{16}+}$$
$$\frac{4.171e49s^{15}-1.02e50s^{14}-2.158e50s^{13}-3.942e50s^{12}-6.187e50s^{11}-8.303e50s^{10}-9.47e50s^{9}-9.11e50s^{8}-7.32e50s^{7}-4.85e50s^{6}-}{7.684e49s^{15}+1.598e50s^{14}+2.897e50s^{13}+4.554e50s^{12}+6.174e50s^{11}+7.171e50s^{10}+7.073e50s^{9}+5.864e50s^{8}+4.034e50s^{7}+2.265e50s^{6}+}$$
$$\frac{2.603e50s^{5}-1.102e50s^{4}-3.536e49s^{3}-8.054e48s^{2}-1.155e48s-7.807e46}{1.017e50s^{5}+3.543e49s^{4}+9.205e48s^{3}+1.67e48s^{2}+1.876e47s+9.757e45}$$

Model reduction functions based on simplified access to Hankel singular value:

100% FP:

$$G_{100,r} = \frac{-0.1482s^3 - 1.417s^2 - 0.841s - 1.121}{s^4 + 2.064s^3 + 2.13s^2 + 1.201s + 0.2044}$$

70% FP:

$$G_{70,r} = \frac{-0.09431s^3 - 2.668s^2 - 1.271s - 3.022}{s^4 + 2.5s^3 + 3.022s^2 + 2.658s + 0.4094}$$

50% FP:

$$G_{50,r} = \frac{-0.06666s^3 - 3.722s^2 - 2.323s - 5.129}{s^4 + 2.81s^3 + 4.523s^2 + 3.962s + 0.6581}$$

30% FP:

$$G_{50,r} = \frac{0.2008s^3 - 8.507s^2 - 7.722s - 6.417}{s^4 + 3.228s^3 + 8.026s^2 + 4.368s + 0.8144}$$

Transfer function of IMC controller $G_c(s)$ at different λ values at 100% FP:

λ = 1:

$$G_c(s) = \frac{-s^4 - 2.064s^3 - 2.13s^2 - 1.201s - 0.2044}{0.1482s^4 + 1.565s^3 + 2.258s^2 + 1.962s + 1.121}$$

λ = 5:

$$G_c(s) = \frac{-0.2s^4 - 0.4128s^3 - 0.426s^2 - 0.2402s - 0.04088}{0.1482s^4 + 1.447s^3 + 1.124s^2 + 1.289s + 0.2242}$$

λ = 10:

$$G_c(s) = \frac{-0.1s^4 - 0.2064s^3 - 0.213s^2 - 0.1201s - 0.02044}{0.1482s^4 + 1.432s^3 + 0.9827s^2 + 1.205s + 0.1121}$$

λ = 20:

$$G_c(s) = \frac{-0.05s^4 - 0.1032s^3 - 0.1065s^2 - 0.06005s - 0.01022}{0.1482s^4 + 1.424s^3 + 0.9118s^2 + 1.163s + 0.05605}$$

References

1. Sun, A.D.; Pu, S.M.; He, Z.X.; Xiao, K.; Sun, P.; Wang, P.; Wei, X. Application of model free active disturbance rejection controller in nuclear reactor power control. *Prog. Nucl. Energy* **2021**, *140*, 103907. [CrossRef]
2. Khan, S.U.-D.; Khan, S.U.-D.; Peng, M. Nuclear power plant systems. In *Nuclear Reactor Technology Development and Utilization*; Woodhead Publishing: Sawston, UK, 2020; pp. 433–471. [CrossRef]
3. Shen, Z.; Shi, J.; Gan, Y.; Sun, B.; Li, Y. Simulation of dryout phenomenon and transient heat transfer performance of the once-through steam generator based on heat transfer partition. *Ann. Nucl. Energy* **2018**, *115*, 268–279. [CrossRef]
4. Lu, J.; Liu, Z.; Zou, Y.; Ding, J. Experimental thermal performance study of molten salt steam generator-superheater with saturated water. *Int. J. Heat Mass Transf.* **2021**, *168*, 120884. [CrossRef]
5. Du, W.; Li, J.; Yuan, B. Dynamic characteristics analysis of a once-through heat recovery steam generator. *Appl. Therm. Eng.* **2020**, *173*, 115155. [CrossRef]
6. Ray, A.; Bowman, H.F. A Nonlinear Dynamic Model of a Once-Through Subcritical Steam Generator. *J. Dyn. Syst. Meas. Control* **1976**, *98*, 332–339. [CrossRef]
7. Ray, A. Dynamic modelling of once-through subcritical steam generator for solar applications. *Appl. Math. Model.* **1980**, *4*, 417–423. [CrossRef]
8. Ray, A. Nonlinear dynamic model of a solar steam generator. *Sol. Energy* **1981**, *26*, 297–306. [CrossRef]
9. Tzanos, P. A Movable Boundary Model for Once-Through Steam Generator Analysis. *Nucl. Technol.* **1988**, *82*, 5–17. [CrossRef]
10. Yi, W.; Li, C.; Wei, R. Comparison of fixed and movable boundary models for once-through steam generator. *Chin. J. Nucl. Sci. Eng.* **2002**, *22*, 314–317. (In Chinese)

11. Ghaffari, V.; Mobayen, S. Robust H_∞ integral controller design for regulation problem of uncertain nonlinear systems with non-zero set-point. *Commun. Nonlinear Sci. Numer. Simul.* **2021**, *107*, 106158. [CrossRef]
12. Jiang, D.; Dong, Z.; Liu, M.; Huang, X. Dynamic Matrix Control for the Thermal Power of MHTGR-Based Nuclear Steam Supply System. *Energies* **2018**, *11*, 2651. [CrossRef]
13. Skålén, S.; Josefsson, F.; Ihrström, J. Nonlinear MPC for grade transitions in an industrial LDPE tubular reactor. *IFAC-PapersOnLine* **2016**, *49*, 562–567. [CrossRef]
14. Qin, Y.; Sun, L.; Hua, Q.; Liu, P. A Fuzzy Adaptive PID Controller Design for Fuel Cell Power Plant. *Sustainability* **2018**, *10*, 2438. [CrossRef]
15. Nohooji, H.R. Constrained neural adaptive PID control for robot manipulators. *J. Frankl. Inst.* **2020**, *357*, 3907–3923. [CrossRef]
16. Garcia, C.E.; Morari, M. Internal model control. II: Design procedure for multivariable systems. *Ind. Eng. Chem. Process Des. Dev.* **1985**, *24*, 472–484. [CrossRef]
17. Kazantzidou, C.; Perez, T.; Donaire, A.; Valentinis, F. Internal Model Control for Rudder Roll Stabilisation and Course Keeping of a Surface Marine Craft. *IFAC-PapersOnLine* **2018**, *51*, 457–462. [CrossRef]
18. Singh, J.; Chattterjee, K.; Vishwakarma, C.B. Two degree of freedom internal model control-PID design for LFC of power systems via logarithmic approximations. *ISA Trans.* **2018**, *72*, 185–196. [CrossRef] [PubMed]
19. Bhattacharjee, A.; Easwaran, A.; Leow, M.K.-S.; Cho, N. Evaluation of an artificial pancreas in in silico patients with online-tuned internal model control. *Biomed. Signal Process. Control* **2018**, *41*, 198–209. [CrossRef]
20. Li, N.L.; Yang, H.; Zhu, W.; Liu, C. A novel grey decision-DE optimized internal model controller for vibration control of nonlinear uncertain aeroelastic blade system. *ISA Trans.* **2020**, *107*, 27–39. [CrossRef] [PubMed]
21. Mesbah, A.; Paulson, J.A.; Braatz, R.D. An internal model control design method for failure-tolerant control with multiple objectives. *Comput. Chem. Eng.* **2020**, *140*, 106955. [CrossRef]
22. Karan, S.; Dey, C.; Mukherjee, S. Simple internal model control based modified Smith predictor for integrating time delayed processes with real-time verification. *ISA Trans.* **2021**, *121*, 240–257. [CrossRef] [PubMed]
23. Schörghuber, C.; Gölles, M.; Reichhartinger, M.; Horn, M. Control of biomass grate boilers using internal model control. *Control Eng. Pract.* **2020**, *96*, 104274. [CrossRef]
24. Wang, P.F.; Chen, Z.; Liao, L.; Wan, J.; Wu, S. A multiple-model based internal model control method for power control of small pressurized water reactors. *Energy* **2020**, *210*, 118527. [CrossRef]
25. Zeng, W.J.; Zhu, W.C.; Hui, T.; Chen, L.; Xie, J.; Yu, T. An IMC-PID controller with Particle Swarm Optimization algorithm for MSBR core power control. *Nucl. Eng. Des.* **2020**, *360*, 110513. [CrossRef]
26. Sun, A.D.; Pu, S.M.; Jiao, W.; Sun, P.; Wei, X. Research on the feedwater control of a multimodule once through steam generator parallel system. *Appl. Therm. Eng.* **2021**, *200*, 117691. [CrossRef]
27. Dittus, F.W.; Boelter, L.M.K. Heat transfer in automobile radiators of the tubular type. In *University of California Publications on Engineering*; University of California: Berkeley, CA, USA, 1930; Volume 2, pp. 443–461.
28. Collier, J.G. *Convective Boiling and Condensation*; McGraw-Jill Book, Co.: New York, NY, USA,, 1972.
29. Chen, J.C. Correlation for Boiling Heat Transfer to Saturated Fluids in Convective Flow. *Ind. Eng. Chem. Process Des. Dev.* **1966**, *5*, 322–329. [CrossRef]
30. Miropolskiy, Z.L. Heat transfer in film boiling of a steam water mixture in steam generating tubes. *Teploenergetika* **1963**, *10*, 49–52.
31. Skupinski, E.; Tortel, J.; Vautrey, L. Determination des coefficients de convection d'un alliage sodium-potassium dans un tube circulaire. *Int. J. Heat Mass Transf.* **1965**, *8*, 937–951. [CrossRef]
32. Wan, J.S. *Research on the Control Systems of the Advanced Small Pressurized Water Reactor*; Xi'an Jiaotong University: Xi'an, China, 2017.
33. Xue, D.; Atherton, D.P. A suboptimal reduction algorithm for linear systems with a time delay. *Int. J. Control* **1994**, *60*, 181–196. [CrossRef]
34. Xue, D. *Computer Aided Design of Control System Using MATLAB Language*, 3rd ed.; Tsinghua University Press: Beijing, China, 2012.